MIT Libraries | DSpace@MIT

MIT Open Access Articles

Modeling reverse osmosis element design using superposition and an analogy to convective heat transfer

The MIT Faculty has made this article openly available. ***Please share*** how this access benefits you. Your story matters.

Citation: Rohlfs, Wilko, Gregory P. Thiel, and John H. Lienhard V. "Modeling Reverse Osmosis Element Design Using Superposition and an Analogy to Convective Heat Transfer." Journal of Membrane Science 512 (August 2016): 38-49.

As Published: http://dx.doi.org/10.1016/j.memsci.2016.03.049

Publisher: Elsevier

Persistent URL: http://hdl.handle.net/1721.1/105436

Version: Author's final manuscript: final author's manuscript post peer review, without publisher's formatting or copy editing

Terms of use: Creative Commons Attribution-Noncommercial-Share Alike

Massachusetts Institute of Technology

Modeling reverse osmosis element design using superposition and an analogy to convective heat transfer

Wilko Rohlfs[a,b,*], Gregory P. Thiel[a,1], John H. Lienhard V[a]

[a]*Department of Mechanical Engineering, Massachusetts Institute of Technology, Cambridge, MA 02139-4307, USA*
[b]*Institute of Heat and Mass Transfer, RWTH Aachen University, Augustinerbach 6, 52056 Aachen, Germany*

Abstract

Accurate models for concentration polarization (CP), the buildup of solutes at the membrane–solution interface in reverse osmosis (RO) channels, are critical for predicting system performance. Despite its empirical success, many modeling approximations employed in the derivation of the oft-used stagnant film model seem to limit the model's applicability to real systems. In addition, many existing models for CP use an average mass transfer coefficient with a local mass transfer driving force, which leads to incorrect predictions for the osmotic pressure at the membrane–channel interface. In this work, we reduce the Zydney-transformed governing equations for solute mass transfer to an analogous convective heat transfer problem. We then apply the principle of superposition to fit solutions from the heat transfer problem to the RO channel boundary conditions, yielding a solution that correctly and consistently combines a local transport coefficient with a local mass transfer driving force. The resulting expression for RO element sizing and rating shows good agreement with experimental data and provides a theoretical basis for CP modeling that captures the characteristic growth of the mass transfer boundary layer not accounted for by many existing, more empirical models. The model has important consequences for the design of RO systems with high permeability membranes, as the decrease in membrane resistance in these systems leads to a relative increase in the importance of CP in system performance.

Keywords: Concentration polarization, Mass transfer, Convection, Membrane transport, Reverse osmosis, Stagnant Film Model

Nomenclature

Roman Symbols

A	Membrane permeability, $\mathrm{m^3/Pa\ s}$
D	Diffusivity, $\mathrm{m^2/s}$
D_h	Hydraulic diameter, $2H$, m
f_os	Modified van 't Hoff coefficient, Pa
H	Channel height, m
h_m	Mass transfer coefficient, $\mathrm{kg/m^2\ s}$
h	Heat transfer coefficient, $\mathrm{W/m^2\ K}$
k	Thermal conductivity, $\mathrm{W/m\ K}$
L	Length, m
j	Mass flux, $\mathrm{kg/m^2\ s}$
n	Wall normal direction
p	Hydraulic pressure, Pa
U	Characteristic streamwise velocity, m/s
U_T	Characteristic streamwise velocity, m/s
U_ω	Characteristic streamwise velocity, m/s
$\vec{u}_\omega$	Velocity for the transformed problem, m/s
$\vec{u}_\mathrm{T}$	Velocity for the analogous HT problem, m/s
$\vec{u}$	Velocity, m/s
v	Permeate volumetric flux, $\mathrm{m^3/m^2 s}$
v_s	Suction velocity, m/s
V_s	Characteristic suction velocity, m/s
w	Mass fraction
x_*	Inverse Graetz Number, $x/(\mathrm{Re\,Sc\,D_h})$

Greek Symbols

α	Thermal diffusivity, $\mathrm{m^2/s}$
δ	Mass transfer boundary layer thickness, m
μ	Dynamic viscosity, $\mathrm{kg/m\ s}$
ξ	Dummy integration variable
π	Osmotic pressure, Pa
ρ	Density, $\mathrm{kg/m^3}$
ω	Pseudo-concentration

*Corresponding author
Email address: rohlfs@wsa.rwth-aachen.de (Wilko Rohlfs)
[1]Joint first author

W. Rohlfs, G.P. Thiel, and J.H. Lienhard V, "Modeling reverse osmosis element design using superposition and an analogy to convective heat transfer," J. Membrane Sci., 512:38-49, 15 August 2016.

Dimensionless Groups

MTU	Mass transfer units, $\Delta pAL/(v_{f,0}H)$
Nu	Nusselt number, hL/k
Pe_L	Peclet number, UL/D
$\mathrm{Pe}_\perp$	Transverse Peclet number, $D_h A(\Delta p - f_{os} w_0)/D$
Pr	Prandtl number, $\mu/\rho\alpha$
Re	Reynolds number, $\rho U D_h/\mu$
RR	Recovery ratio, $2\bar{v}L/(v_{f,0}H)$
Sc	Schmidt number, $\mu/\rho D$
Sh	Sherwood number, $h_\mathrm{m} D_h/D$
$\widetilde{\mathrm{Sh}}$	Local Sherwood number for spatially varying permeate flux
SR_f	Feed osmotic pressure ratio

Subscripts

0	Inlet
b	Bulk
f	Feed
L	Outlet
n	Wall normal direction
p	Permeate
n	Wall tangential direction
w	Wall, i.e., membrane surface

1. Introduction

In reverse osmosis (RO), the rejection of solutes by the membrane causes a buildup of solutes at the membrane surface, which increases the local osmotic pressure and retards water flux through the membrane. This phenomenon is known as concentration polarization (CP). Accurate prediction of the osmotic pressure—or equivalently, the solute concentration—at the membrane surface in RO systems is thus a critical problem for predicting the permeate flux, which in turn is essential for membrane sizing and techno-economic optimization. Good models for CP are even more important in systems using ultrapermeable membranes (UPMs) [1–3], as the higher permeability leads to a relatively larger mass transfer resistance from CP. In addition, high solute concentrations at the membrane surface can lead to fouling or scaling, which reduce the effective membrane surface area and increase maintenance cost. With improved predictability of solute concentrations at the membrane, such issues can be better prevented.

Almost fifty years ago, Michaels [4] applied the stagnant film model to specify the solute concentration at the membrane surface as a function of the bulk concentration and the permeate flux. Despite its analytical simplicity, the classic stagnant film approach involves several limitations, including the use of a conductive-like mass transfer coefficient and a wall-normal velocity that is invariant through the mass transfer boundary layer. The details of the approximations used to develop of the stagnant film model will be presented in Sec. 2.

Many improved analyses of concentration polarization in membrane channels are based on simplified mass transfer equations allowing for analytical or semi-analytical solutions of the problem [5–9]. However, most of these models are still limited by modeling approximations such as a constant permeate flux through the boundary layer and an axially invariant permeate flux. Further, many models rely on empirical correlations for the mass transfer coefficient, and/or incorrectly link an average mass transfer coefficient with a local driving force. Numerical methods [10–13] have been applied to overcome the drawbacks associated with the simplified models, but are computationally intensive and can be difficult to generalize.

The contribution of this article is threefold. First, following the approach of Zydney [14], we transform the governing species conservation equations to derive a model for concentration polarization that mathematically resembles the stagnant film, but which relaxes several of the often-stated modeling approximations. Second, we show how, under certain conditions, mass transfer coefficients for the film can be obtained by analogy to convective heat transfer, a subject for which a vast theoretical and experimental literature is available. Finally, we use the principle of superposition to develop a new model for membrane performance (recovery ratio, or permeate flux) as a function of operating conditions, system geometry, and mass transfer coefficients. The latter are obtained from constant wall flux solutions to the governing transport equations. Results from the model are benchmarked against measurements, existing models in the literature, and solutions from direct numerical simulation. The results show better predictive performance at high degrees of concentration polarization, as would be found in systems with UPMs.

2. Development of the Stagnant Film Model

A stagnant film (Fig. 1) assumes that there are no axial variations in the mass transfer boundary layer (MTBL) thickness, the solute concentration, and the solvent flux, leading to a 1-D problem. Application of the stagnant film model to concentration polarization was first presented by Michaels [4] and is derived by balancing the convective solute flux ($\rho v_n w$) towards the membrane with the counter-diffusive flux of solute away from the membrane that results from membrane solute

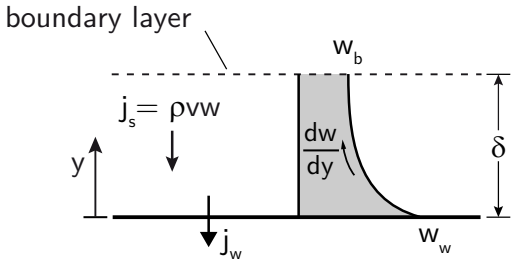

Figure 1: As the solute is pulled convectively towards the wall, j_s, under the influence of the solvent suction through the wall, j_w, a counter-diffusive flux of the solute back towards the bulk develops. In a stagnant film, all properties vary only in the y-coordinate.

rejection. Axial variations in both the permeate velocity and the solute concentration gradient are neglected, resulting in the following equation for species conservation:

$$\rho v_n w - \rho D \frac{dw}{dn} = 0, \tag{1}$$

where n is the unit vector that points normal to the membrane surface into the solution and $-v_n$ is the permeate velocity, or volumetric flux. The mixture density is denoted ρ, w is the solute mass fraction, and D is the diffusivity of the solute in the solvent. Although the typical RO feed may contain multiple solutes, here we lump them together, modeling solute diffusivity with a single value D.

Taking the permeate velocity as constant through the MTBL allows Eq. (1) to be integrated across the MTBL thickness δ, yielding the proportionality between the permeate flux and the logarithm of the bulk-to-wall concentration ratio that is the hallmark of the stagnant film model:

$$v_n = \frac{D}{\delta} \ln\left(\frac{w_\mathrm{w}}{w_\mathrm{b}}\right). \tag{2}$$

The term D/δ is the mass transfer conductance based on the logarithmic concentration driving force, and is constant in the stagnant film model.

However, in long but narrow membrane channel flows, the concentration boundary layer can grow to cover a significant portion of the—or even the entire—channel height. Some key limitations of the stagnant film model mentioned in literature (see, e.g., [9, 15] for a description), revolve mostly around the simplification to 1-D, and include:

- neglecting axial convection near the membrane surface,
- neglecting the influence of the permeate flux on the boundary layer thickness,
- neglecting axial variation in the permeate flux,
- assuming fully developed velocity and concentration profiles.

In spite of these limitations, however, models that use a logarithmic driving force to characterize the diffusion of solute across the MTBL have achieved considerable predictive success. In the following section, we follow the approach of Zydney [14], who showed that the mathematical form of the stagnant film model, albeit with a different mass transfer coefficient, can be derived using far fewer approximations than those listed above.

3. Zydney's Transformation and the Analogous Heat Transfer Problem

3.1. Transformation Using a Pseudo-Concentration

Zydney [14] uses a transformation of variables to show that the logarithmic concentration driving force that characterizes the stagnant film model is the correct driving force for the coupled convective and diffusive transport near the membrane surface. In this section, we adhere to Zydney's general idea [14] that validates the form of the stagnant film model by transforming the transport equation of a passive scalar (the solute). For simplicity, but without loss of generality, the governing equations are presented in two dimensions. For a spatially-invariant density, the species conservation equation can be written in terms of solute mass fraction w, which yields

$$\frac{\partial w}{\partial t} + u_x \frac{\partial w}{\partial x} + u_y \frac{\partial w}{\partial y} = D\left(\frac{\partial^2 w}{\partial x^2} + \frac{\partial^2 w}{\partial y^2}\right), \tag{3}$$

where $\vec{u} = (u_x, u_y)$ is the velocity field and D is the mass diffusivity of the solute in the solution. At the permeable boundary, i.e., the membrane surface, the no solute flux boundary condition is

$$-\rho D \frac{\partial w}{\partial n} - \rho w v_n = 0. \tag{4}$$

A non-zero term on the right hand side of Eq. (4) can be added to account for solute permeation through the membrane, but we will restrict ourselves to the case of full solute rejection for simplicity.

Along the impermeable boundary or a symmetry plane, there is no solute flux:

$$\frac{\partial w}{\partial n} = 0. \tag{5}$$

For the case that density changes by the solute/solvent mixture are small (i.e., $D\rho/Dt = 0$), the x and y momentum equations read, respectively

$$\frac{\partial u_x}{\partial t} + u_x\frac{\partial u_x}{\partial x} + u_y\frac{\partial u_x}{\partial y} = -\frac{1}{\rho}\frac{\partial p}{\partial x} + \frac{\mu}{\rho}\left(\frac{\partial^2 u_x}{\partial x^2} + \frac{\partial^2 u_x}{\partial y^2}\right), \tag{6}$$

$$\frac{\partial u_y}{\partial t} + u_x\frac{\partial u_y}{\partial x} + u_y\frac{\partial u_y}{\partial y} = -\frac{1}{\rho}\frac{\partial p}{\partial y} + \frac{\mu}{\rho}\left(\frac{\partial^2 u_y}{\partial x^2} + \frac{\partial^2 u_y}{\partial y^2}\right), \tag{7}$$

which, together with the continuity equation,

$$\frac{\partial u_x}{\partial x} + \frac{\partial u_y}{\partial y} = 0, \tag{8}$$

describe the fluid motion. Normal to the membrane surface, the boundary condition is

$$u_n = -v_n, \tag{9}$$

and the boundary condition for the impermeable wall is simply $u_n = 0$. Tangent to the membrane surface and the impermeable wall, the no slip boundary condition applies:

$$u_t = 0. \tag{10}$$

The solution to these momentum and species conservation equations differs from solutions for momentum and energy equations in typical internal convective flow problems only by the boundary condition at the permeable wall. The impact of this boundary condition is significant owing to high mass transfer rates through the membrane in RO membrane channels. Consequently, the analogy between heat and mass transfer that is applied to low-rate mass transfer problems cannot be directly applied to RO.

A possible way to solve the problem at hand is by introducing a pseudo-concentration, ω, as shown by Zydney [14] and also used in other studies [16]. For $w > 0$, the pseudo-concentration is defined by the relationship

$$\frac{\partial \omega}{\partial w} = \frac{1}{w}. \tag{11}$$

Substituting the pseudo-concentration into the solute transport equation reveals an equation of similar mathematical form to the original, but with two additional terms:

$$\frac{\partial \omega}{\partial t} + u_x\frac{\partial \omega}{\partial x} + u_y\frac{\partial \omega}{\partial y} = D\left(\frac{\partial^2 \omega}{\partial x^2} + \frac{\partial^2 \omega}{\partial y^2} + \underbrace{\left(\frac{\partial \omega}{\partial x}\right)^2 + \left(\frac{\partial \omega}{\partial y}\right)^2}_{\text{additional terms}}\right). \tag{12}$$

Along the membrane surface, the transformed boundary condition is

$$-D\frac{\partial \omega}{\partial n} = v_n. \tag{13}$$

At the impermeable wall or the symmetry plane, the boundary condition becomes

$$\frac{\partial \omega}{\partial n} = 0. \tag{14}$$

If we define a mass transfer coefficient based on the pseudo-concentration in the usual manner,

$$h_\mathrm{m} = \frac{-D\left.\frac{\partial \omega}{\partial n}\right|_\mathrm{w}}{(\omega_\mathrm{w} - \omega_\mathrm{b})}, \tag{15}$$

the boundary condition prescribed by Eq. (13) reduces to none other than a mass transfer coefficient times a logarithmic concentration driving force, mirroring the mathematical form of the stagnant film model:

$$v_n = -D\left.\frac{\partial \omega}{\partial n}\right|_\mathrm{w} = h_\mathrm{m}\left(\omega_\mathrm{w} - \omega_\mathrm{b}\right) = h_\mathrm{m}\ln\left(\frac{w_\mathrm{w}}{w_\mathrm{b}}\right). \tag{16}$$

This is a key finding of Zydney [14], and it explains the empirical success of the stagnant film model in describing concentration polarization in RO channels, despite the modeling approximations required in its development. The logarithmic concentration driving force appears solely as a result of the solute-flux boundary condition and the transformation of the concentration variable. Consequently, mass transfer coefficients defined by Eq. (15)—without reducing the problem to 1-D—can accurately describe solute mass transfer in RO channels where MTBL growth can be significant.

Although the pseudo-concentration transformation increases the complexity of the solute transport equation by introducing two new terms, the boundary condition at the membrane surface collapses to a simpler Neumann boundary condition, where the counter-diffusion gradient depends only on the local permeate flux. Note that the momentum equations and boundary conditions are not affected by the transformation, such that the permeable wall boundary condition still influences the velocity field. Rearranging equation (12) into a more suggestive form yields

$$\frac{\partial \omega}{\partial t} + \underbrace{\left(u_x - D\frac{\partial \omega}{\partial x}\right)}_{u_{\omega,x}}\frac{\partial \omega}{\partial x} + \underbrace{\left(u_y - D\frac{\partial \omega}{\partial y}\right)}_{u_{\omega,y}}\frac{\partial \omega}{\partial y} = D\left(\frac{\partial^2 \omega}{\partial x^2} + \frac{\partial^2 \omega}{\partial y^2}\right). \tag{17}$$

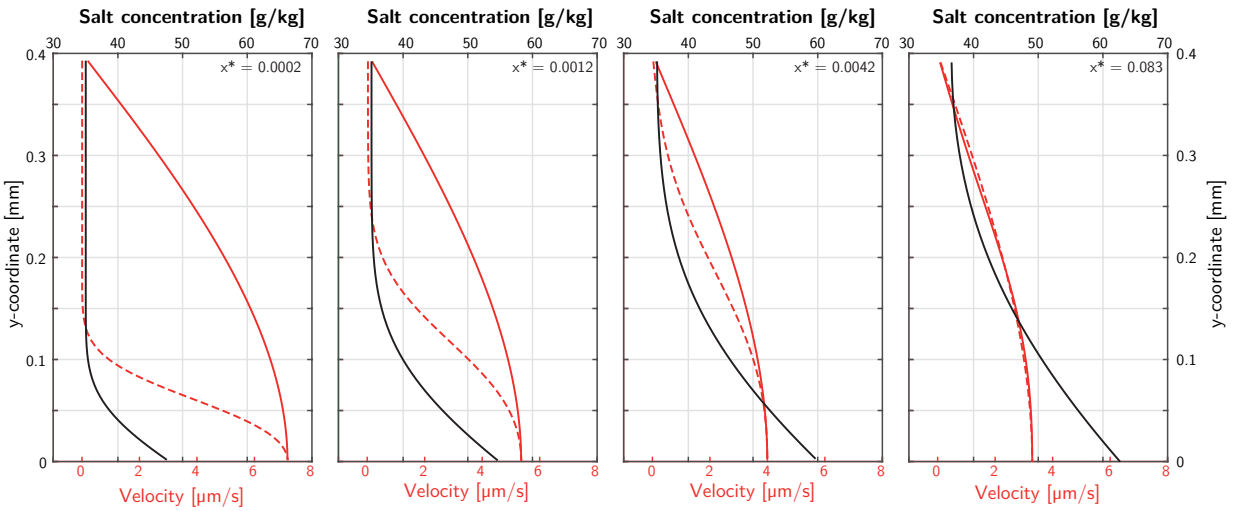

Figure 2: Local profiles of the pseudo-concentration (black line), the wall-normal velocity u_y (red solid line), and the correction to the pseudo-velocity v_y (red dashed line) for an inlet Reynolds number of Re = 32, channel dimensions $H = 0.8$ mm, $L = 1$ m, membrane permeability $A = 1$ L/m^2 h bar, a hydraulic pressure $\Delta p = 65$ bar, and an NaCl solution with inlet salinity $w_0 = 35$ g/kg.

Written as such, equation (17) shows that the transformed problem for the pseudo-concentration ω with the impermeable wall boundary condition is analogous to the well-known convective heat transfer problem with an imposed temperature gradient at the wall if the pseudo-velocity field described by $u_{\omega,x}$ and $u_{\omega,y}$ is equal to the velocity field of the heat transfer problem $u_{\mathrm{T},x}$ and $u_{\mathrm{T},y}$. In such cases, solutions for the local transport number in convective heat transfer can be used to calculate h_m in RO channels. (The full, transformed governing equations are given in Appendix C)

3.2. The Analogous Convective Heat Transfer Problem

Now we seek to show how solutions to internal convective heat transfer problems can be used to solve the transformed governing equations discussed above. For a perfect analogy, the governing equations and boundary conditions must be identical; here the boundary conditions are identical, but the governing equations are only approximately identical, as follows.

The two velocity fields $\vec{u}_\omega$ and $\vec{u}_\mathrm{T}$ are identical if both the governing equations and the boundary conditions match. Strictly identical are the boundary conditions for the permeable wall, where

$$u_n = -v_n = D\frac{\partial \omega}{\partial n}, \tag{18}$$

which, in the transformed problem leads to $u_{\omega,n} = 0$. This is identical to the zero wall-normal velocity b.c. in the convective heat transfer problem, $u_{\mathrm{T},n} = 0$. The velocity field boundary condition at the impermeable wall or symmetry plane is also identical.

In order for the governing equations (mass, momentum, and species conservation) to be approximated by the convective heat transfer problem, $\vec{u}_\omega$ should be equal to $\vec{u}_\mathrm{T}$. Three conditions, as quantified by three dimensionless groups, must be fulfilled for this equivalence to hold: (1) negligible axial diffusion; (2) small changes in u_x; and (3) equality of the suction velocity and the counterdiffusion velocity throughout the MTBL.

Along the x-coordinate, the first condition is fulfilled so long as $u_x \gg -D(\partial\omega/\partial x)$. For the scalings $u_x \sim U$, and $(\partial\omega/\partial x) \sim \Delta\omega/L$, we see this is fulfilled when

$$\frac{D\Delta\omega}{UL} \ll 1, \tag{19}$$

or

$$\frac{\ln(w_L/w_0)}{\mathrm{Pe}_L} \ll 1, \tag{20}$$

which is true for typical RO elements. The axial Peclet number, $\mathrm{Pe}_L = UL/D$, and is generally around 10^7 to 10^8 for typical salt solutions and crossflow velocities. For a 15% element recovery, $\ln(w_L/w_0) \approx 0.2$, so the LHS of Eq. (20) is between about 10^{-8} and 10^{-9} and the condition is fulfilled.

The second condition, a near-constant x-coordinate

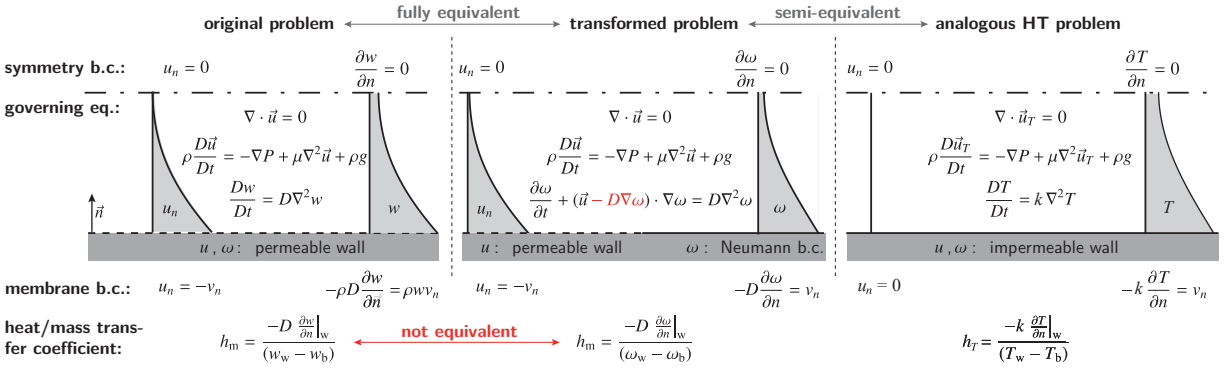

Figure 3: Governing equations and boundary conditions for the original problem in concentration w, the transformed problem in psuedo-concentration ω, and the analogous heat transfer problem in T. Equivalence of the original and transformed problem is complete. The analogy to convective heat transfer holds under the conditions where the velocity field is not significantly impacted by the permeate flux and axial diffusion.

velocity field, is fulfilled for small recovery ratios, i.e.,

$$\frac{Q_p}{Q_{f,0}} \ll 1, \tag{21}$$

where Q_p is the volume flow rate of permeate, and $Q_{f,0}$ is the inlet volume flow rate of feed. This is generally fulfilled for single RO elements, which typically have recovery ratios near 15% or less. (Nevertheless, model predictions show good agreement with the full problem solution beyond this limit, as discussed in Sec. 5.)

Along the y-coordinate, $u_{\omega,y}$ is equivalent to the velocity field in the absence of suction, $u_{\mathrm{T},y}$, under the following conditions. First, if we neglect the inertia terms in the y-direction momentum equation, it becomes linear, so we can superpose solutions. Thus, we can write $u_y = u_{\mathrm{T},y} + v_\mathrm{s}$, where v_s is the velocity associated with suction at the boundary. When v_s is approximately equal to the counter-diffusion flux $D(\partial\omega/\partial y)$, $u_{\omega,y} = u_{\mathrm{T},y} = u_y - D(\partial\omega/\partial y)$. Thus, when $v_\mathrm{s} \approx D(\partial\omega/\partial y)$, $u_{\omega,y} \approx u_{\mathrm{T},y}$. We check this approximate equality by scaling the terms as follows: $v_\mathrm{s} \sim V_\mathrm{s}$, and $D(\partial\omega/\partial y) \sim D\Delta\omega/\delta$. Thus, the two terms are approximately equal when

$$V_\mathrm{s} \sim \frac{D\Delta\omega}{\delta}, \tag{22}$$

where δ is the MTBL thickness. From scaling arguments on the continuity equation (assuming the condition specified by Eq. (20) is also fulfilled),

$$\frac{U}{L} \sim \frac{U_{\mathrm{T},y} + V_\mathrm{s}}{H}, \tag{23}$$

where we have taken the hydrodynamic length scale in y to be equal to the channel height, as the hydrodynamic entrance length is typically $< 1\%$ of the channel length. Solving for V_s and substituting into Eq. (22), with some rearrangement, the condition for the equivalence of V_s and the counterdiffusion flux becomes

$$\frac{\frac{UH\delta}{DL\Delta\omega}}{1 + \frac{U_{\mathrm{T},y}\delta}{D\Delta\omega}} \sim 1. \tag{24}$$

For the case where the y velocity in the absence of suction is zero, i.e., for a fully developed duct flow, the condition above reduces to

$$\mathrm{Pe}_L^{1/2} \frac{H}{L} \ln\left(\frac{w_0}{w_L}\right)\left(\frac{x}{L}\right)^{1/2} \sim 1, \tag{25}$$

where we have used the well-established boundary layer scaling law $\delta \sim x(\mathrm{Re}\cdot\mathrm{Sc}\cdot x/D_h)^{-1/2}$ [17] to describe the growth of the MTBL thickness. For typical RO channels, this is fulfilled for a portion of the channel, but not the entire channel, as seen in Fig. 2, which shows the crosswise concentration profile in a mass transfer channel at different dimensionless locations $x_* = x/(D_\mathrm{h}\cdot\mathrm{Re}\cdot\mathrm{Sc})$. A symmetry boundary condition is applied at the channel half-height ($y = 0.4$ mm).

At all x_*, the wall-normal velocity u_y and the correction to the velocity, $D(\partial\omega/\partial y)$, coincide at the channel wall, such that the no-flux boundary condition for the pseudo-velocity $u_{\omega,n} = 0$ is fulfilled. In the developing region of the MTBL, the two velocity profiles diverge towards the channel center. However, beyond the inlet region, the velocity profiles coincide. Figure 3 summarizes the equations valid in the original, transformed, and analogous convective heat transfer problem.

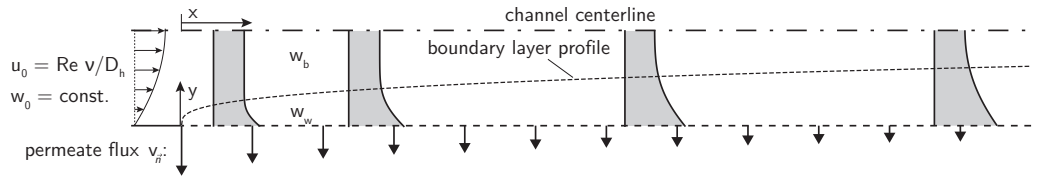

Figure 4: Schematic of a reverse osmosis channel. The two membrane walls on both sides introduce symmetry boundary condition. The grey highlighted areas illustreate concentration profiles at different locations.

4. Model Development

In this section, we develop a model for RO element sizing and rating using the principle of superposition and the analogy between mass transfer in RO channels and convective heat transfer, as described above. To do so, we superpose constant wall heat flux solutions from heat transfer theory to match the varying wall flux b.c. in RO channels. We first present the development of an expression for the permeate flow rate as a function of geometry and inlet conditions, and generalize the expression using dimensionless parameters to yield an improved effectiveness (ε)–MTU relationship.

4.1. Dimensional Model

We approximate the feed channel in a spiral-wound RO element as a 2D channel, as shown in Fig. 4: as the MTBL develops, the effect of CP increases, and the permeate flux is reduced. Based on the definition of the Sherwood number

$$\mathrm{Sh} = \frac{h_\mathrm{m} D_\mathrm{h}}{D}, \tag{26}$$

and the transformed no salt flux b.c. (Eq. 13), the local permeate flux can be written

$$v(x) = \frac{D}{D_\mathrm{h}} \widetilde{\mathrm{Sh}}(x) \ln\left(\frac{w_\mathrm{w}}{w_\mathrm{b}}\right), \tag{27}$$

where $\widetilde{\mathrm{Sh}}(x)$ is in general the local Sherwood number obtained for the streamwise-varying Neumann boundary condition at the permeable walls, Eq. (13). Note that the equation above is equivalent to Eq. (16), replacing the local mass transfer coefficient by the local Sherwood number.

Because the governing transport equation is linear, sums of solutions are also solutions—this is the principle of superposition. Under this principle, convective heat transfer problems with arbitrary variations in wall heat flux can be solved by weighted integration of uniform heat flux solutions [18, 19]. An illustrative example of the principle is given in Appendix A, which results in an explicit expression for the dimensionless heat transfer coefficient (Eq. (A.7)).

By analogy to Eq. (A.7), the local Sherwood number at the position x for $v(x) = v_0 + f(x)$ is given by

$$\widetilde{\mathrm{Sh}}(x) = \frac{\overbrace{v_0 + \int_0^x \frac{\partial v}{\partial \xi} d\xi}^{v(x)}}{\frac{v_0}{\mathrm{Sh}(x)} + \int_0^x \frac{\partial v(\xi)}{\partial \xi} \frac{1}{\mathrm{Sh}(x-\xi)} d\xi}. \tag{28}$$

The equation above states that the local Sherwood number at position x is a result of the history of the imposed boundary condition from the channel entrance up to the position x. For typical expressions like $\mathrm{Sh} = f(\mathrm{Re}, \mathrm{Sc})$ taken from solutions to the analogous HT problem, Sc and Re are generally treated as constants, even though Re decreases in streamwise direction due to the permeate mass loss in RO channels. (See Sec. 3.2 for the validity of this approximation.) Combining equations (27) and (28) and dividing both sides by $v(x)$ yields

$$\frac{v_0}{\mathrm{Sh}(x)} + \int_0^x \frac{\partial v}{\partial \xi} \frac{1}{\mathrm{Sh}(x-\xi)} d\xi = \frac{D}{D_\mathrm{H}} \ln\left(\frac{w_\mathrm{w}}{w_\mathrm{b}}\right). \tag{29}$$

The bulk solute concentration w_b increases in streamwise direction (x) as solvent permeates through the membrane and out of the feed channel. For perfect solute rejection, solute is conserved in the feed channel, and

$$w_\mathrm{b} = w_0 \frac{1}{1 - \int_0^x \frac{2v(\xi)}{H v_{f,0}} d\xi}, \tag{30}$$

where w_0 is the bulk concentration at the inlet of the membrane channel. The factor of two appears as permeate flows out of the top and bottom of the feed channel.

From solution–diffusion theory [20], the local permeate flux is specified by

$$v(x) = A\left(\Delta p - \pi_\mathrm{w}\right), \tag{31}$$

where we have neglected the retarding influence of the osmotic pressure of the permeate stream, consistent with our no solute permeation approximation. Using van 't Hoff's linear law for osmotic pressure ($\pi = f_{os}\, w$), the permeate flux can be rewritten in terms of the salt concentration at the membrane surface, w_{w}:

$$v(x) = A\left(\Delta p - f_{\mathrm{os}} w_{\mathrm{w}}\right). \tag{32}$$

Substituting Eq. (30) into Eq. (29), solving for w_{w}, and inserting the result into Eq. (32) yields an expression for the local permeate flux as a function of inlet conditions, geometry, and the local Sh:

$$v(x) = A\Delta p - \frac{A f_{\mathrm{os}} w_0}{1 - \int_0^x \frac{2v(\xi)}{H v_{f,0}} d\xi} \exp\left[\left(\frac{v_0}{\mathrm{Sh}(x)} + \int_0^x \frac{\partial v}{\partial x} \frac{1}{\mathrm{Sh}(x-\xi)} d\xi\right) \frac{D_{\mathrm{h}}}{D}\right]. \tag{33}$$

The net permeate flow through the membrane surface per unit length, $\bar{v}L$, is obtained by integrating the above expression over the entire channel length L:

$$\bar{v}L = \int_0^L \left\{ A\Delta p - \frac{A f_{\mathrm{os}} w_0}{1 - \int_0^x \frac{2v(\xi)}{H v_{f,0}} d\xi} \exp\left[\left(\frac{v_0}{\mathrm{Sh}(x)} + \int_0^x \frac{\partial v}{\partial x} \frac{1}{\mathrm{Sh}(x-\xi)} d\xi\right) \frac{D_{\mathrm{h}}}{D}\right] \right\} dx. \tag{34}$$

4.2. Dimensionless Model

We now proceed to rewrite the above relationship for the permeate flow in dimensionless form to illustrate the major design trade-offs between geometry, inlet conditions, and permeate production. With some manipulation, the equation above in a dimensionless fashion yields

$$\frac{\bar{v}L}{v_{f,0} H} = \frac{\Delta p A L}{v_{f,0} H} - \frac{A f_{\mathrm{os}} w_0 L}{v_{f,0} H} \times \int_0^1 \left(\frac{\exp\left[\left(\frac{1}{\mathrm{Sh}(x)} + \int_0^x \frac{\partial v / v_0}{\partial \xi} \frac{1}{\mathrm{Sh}(x-\xi)} d\xi\right) \frac{D_{\mathrm{h}} v_0}{D}\right]}{1 - \int_0^x \frac{2v(\xi)}{H v_{f,0}} d\xi} \right) d\left(\frac{x}{L}\right). \tag{35}$$

Examination of Eq. (35) reveals the following dimensionless quantities, the first three of which are as defined by Banchik et al. [21]:

$$\mathrm{MTU} = \frac{\Delta p A L}{v_{f,0} H}, \tag{36}$$

$$\mathrm{RR} = \frac{2\bar{v}L}{v_{f,0} H}, \tag{37}$$

$$\mathrm{SR_f} = \frac{f_{\mathrm{os}} w_0}{\Delta p}, \tag{38}$$

$$\mathrm{Pe}_{\perp} = \frac{D_{\mathrm{h}} A \left(\Delta p - f_{\mathrm{os}} w_0\right)}{D}. \tag{39}$$

The mass transfer units (MTU) is a dimensionless mass exchanger size analogous to the number of transfer units (NTU) commonly used for heat exchangers. The feed stream osmotic pressure ratio, SR_f, scales the inlet osmotic pressure to the hydraulic pressure difference; in effect, it is a dimensionless measure of the inlet flux. The recovery ratio (RR), here defined volumetrically, is the volume flow rate of permeate per unit feed. The maximum recovery ratio that can be obtained in a system is limited by the osmotic pressure ratio $\mathrm{RR}_{\mathrm{max}} = 1 - \mathrm{SR}_f$ [21]. Finally, the transverse Peclet number, $\mathrm{Pe}_{\perp}$, falls out of the mass transfer expression, and scales the inlet permeate flux against the counter-diffusive solute flux. Together with Sh, $\mathrm{Pe}_{\perp}$ scales the influence of CP. If the Peclet number is high, CP becomes more important in the desalination process.

Inserting the dimensionless variables into Eq. (35), RR can be expressed as a function of MTU, $\mathrm{SR_f}$, $\mathrm{Pe}_{\perp}$, and the local Sh as

$$\mathrm{RR} = 2 \cdot \mathrm{MTU} \times \left[1 - \mathrm{SR}_f \times \int_0^1 \left(\frac{\exp\left[\mathrm{Pe}_{\perp}\left(\frac{1}{\mathrm{Sh}(x)} + \int_0^x \frac{\partial v / v_0}{\partial \xi} \frac{1}{\mathrm{Sh}(x-\xi)} d\xi\right)\right]}{1 - \int_0^x \frac{d\mathrm{RR}}{d\xi} d\xi} \right) d\left(\frac{x}{L}\right)\right], \tag{40}$$

where the integrand $2v/(Hv_{f,0}) = d\mathrm{RR}/dx$. The numerator of the outer integrand encapsulates the effect of concentration polarization using superposition; as this term goes to unity, the expression reduces to Eq. (11) in [21], as shown in Appendix B.

Equations (34) and (40) can be integrated numerically using a variety of schemes [22], including a simple Riemann sum. Because $v(x)$ is a function of $v'(x) = \partial v/\partial x$, $v'(0)$ is required to start the numerical integration. By Eq. (32), $v'(0) = -A f_{os} w'_w(0)$. But at $x = 0$, the MTBL thickness is zero, and so $w_w = w_b$, or equivalently $\pi_w = \pi_b$. Consequently, the evolution of w_w at $x = 0$ is given by differentiating Eq. (30) with respect to x, which yields

$$\left.\frac{\partial v}{\partial x}\right|_{x=0} = -A f_{os} \left.\frac{dw_w}{dx}\right|_{x=0} = -A f_{os} w_0 \frac{2v_0}{H v_{f,0}}. \tag{41}$$

The present modeling approach has two distinct advantages over traditional approaches that use stagnant film theory with an average mass transfer coefficient. First, by combining Zydney's transformation and the analogy to convective heat transfer, we have a well-founded theoretical basis for CP in RO channels. In contrast to empirically derived correlations of the form $\mathrm{Sh} = C \cdot \mathrm{Re}^{\alpha} \cdot \mathrm{Sc}^{\beta}$, solutions to and scaling laws from well-known laminar flow, constant flux heat transfer problems can describe the solute mass transfer phenomena under robust, quantitative constraints (see Sec. 3.2). Moreover, the present model correctly combines a local mass transfer coefficient with a local mass transfer driving force, ensuring theoretical consistency and therefore improved predictability. Second, by accounting for a varying mass transfer coefficient along the channel length, the model allows for an optimization of channel geometry and hydrodynamic design. Such an optimization is not possible with models that lump mass transfer characteristics into a single, averaged coefficient.

4.3. Effectiveness Relationship

By introducing one additional variable, the maximum recovery ratio, we can manipulate the RR–MTU model into the desired ε–MTU relationship. Effectiveness ε is defined as the ratio of the total permeate flow rate to the maximum possible permeate flow rate for the given hydraulic pressure, Δp, and the inlet osmotic pressure, $f_{\mathrm{os}} w_0$,

$$\varepsilon = \frac{\mathrm{RR}}{\mathrm{RR}_{\max}} = \frac{\mathrm{RR}}{1 - \mathrm{SR}_f}. \tag{42}$$

A detailed derivation of effectiveness is provided in Banchik et al. [21]. For large membrane sizes (equivalently, large MTU), ε approaches one. In ε–MTU terms, Eq. (40) becomes

$$\varepsilon = \frac{2 \cdot \mathrm{MTU}}{1 - \mathrm{SR}_f} \times \Big[1 - \mathrm{SR}_f \times \int_0^1 \left(\frac{\exp\left[\mathrm{Pe}_{\perp}\left(\frac{1}{\mathrm{Sh}(x)} + \int_0^x \frac{\partial v/v_0}{\partial \xi} \frac{1}{\mathrm{Sh}(x-\xi)} d\xi\right)\right]}{1 - \int_0^x \frac{d\mathrm{RR}}{d\xi}\, d\xi} \right) d\left(\frac{x}{L}\right) \Big]. \tag{43}$$

The MATLAB code provided in the supplementary material (REFERENCE BY EDITOR) can be used to obtain solutions to Eq. (43).

5. Results and Validation

To evaluate the model's predictive potential, we use a Graetz solution for the local Sh and benchmark the results for RR and ε against: (1) direct numerical simulation; (2) a typical modeling approach that uses a constant Sh; and (3) experimental data.

5.1. Effectiveness–MTU Diagram

To integrate Eq. (43) we require an expression for Sh. From classical scaling laws, the hydrodynamic entry length is much smaller ($\lesssim$ 2%) than typical element lengths, so we assume a developed velocity profile at the channel inlet. However, owing to the high Sc that characterizes many salt solutions (typically near 700 [23]), the mass transfer entry length is much larger than the hydrodynamic entry length, and approaches element length scales. Consequently, we cannot neglect developing flow effects in the MTBL.

Solutions to the problem of a thermally developing, hydrodynamically developed duct flow, the Graetz-Lévêque Problem, are well-known [17, 24]. Applying the analogy described in Sec. 3.2, we take the approximation to the Graetz solution [19] for a constant second-kind b.c. (uniform wall heat flux, H), replacing the Nusselt number, Nu, by Sh and the Prandtl number, Pr, by Sc to find

$$\mathrm{Sh} = \begin{cases} 1.490 x_*^{-1/3}, & \text{for } x_* \le 0.0002, \\ 1.490 x_*^{-1/3} - 0.4, & \text{for } 0.0002 < x_* \le 0.001 \\ 8.235 + 8.68(10^3 x_*)^{-0.506} & \\ \quad \times \exp(-164 x_*), & \text{for } x_* > 0.001, \end{cases} \tag{44}$$

where x_* is the inverse Graetz number $x_* = x/(D_{\mathrm{h}} \cdot \mathrm{Re} \cdot \mathrm{Sc})$. For large values of x_*, the correlation limits to 8.235, the value for a fully developed, 2-D channel flow. Equation (44) is valid for laminar flow, which is the typical hydrodynamic regime in RO. A plot of Eq. (44) is shown in red in Fig. 5, and display the characteristic 1/3 Graetz scaling for developing laminar flow.

In the present study, we choose to model a channel without spacers. However in a recent study by the authors [25], spacers are found not to influence the developing character of the concentration boundary layer if the channel flow is stationary, i.e. without periodic or non-periodic oscillations. Thus, in the Graetz number scaling, spacers will only affect the coefficient on x_*, and not the characteristic exponent (1/3) in the developing region or the asymptote in the developed region.

With the above expressions for Sh, we can integrate Eq. (43), yielding the results shown in Fig. 6. As expected, CP has a greater effect in decreasing ε as $\mathrm{Pe}_{\perp}$ increases. A larger $\mathrm{Pe}_{\perp}$ (driven, e.g., by a higher membrane permeability) corresponds to a higher initial flux, which increases the reactive counterdiffusion flux, or

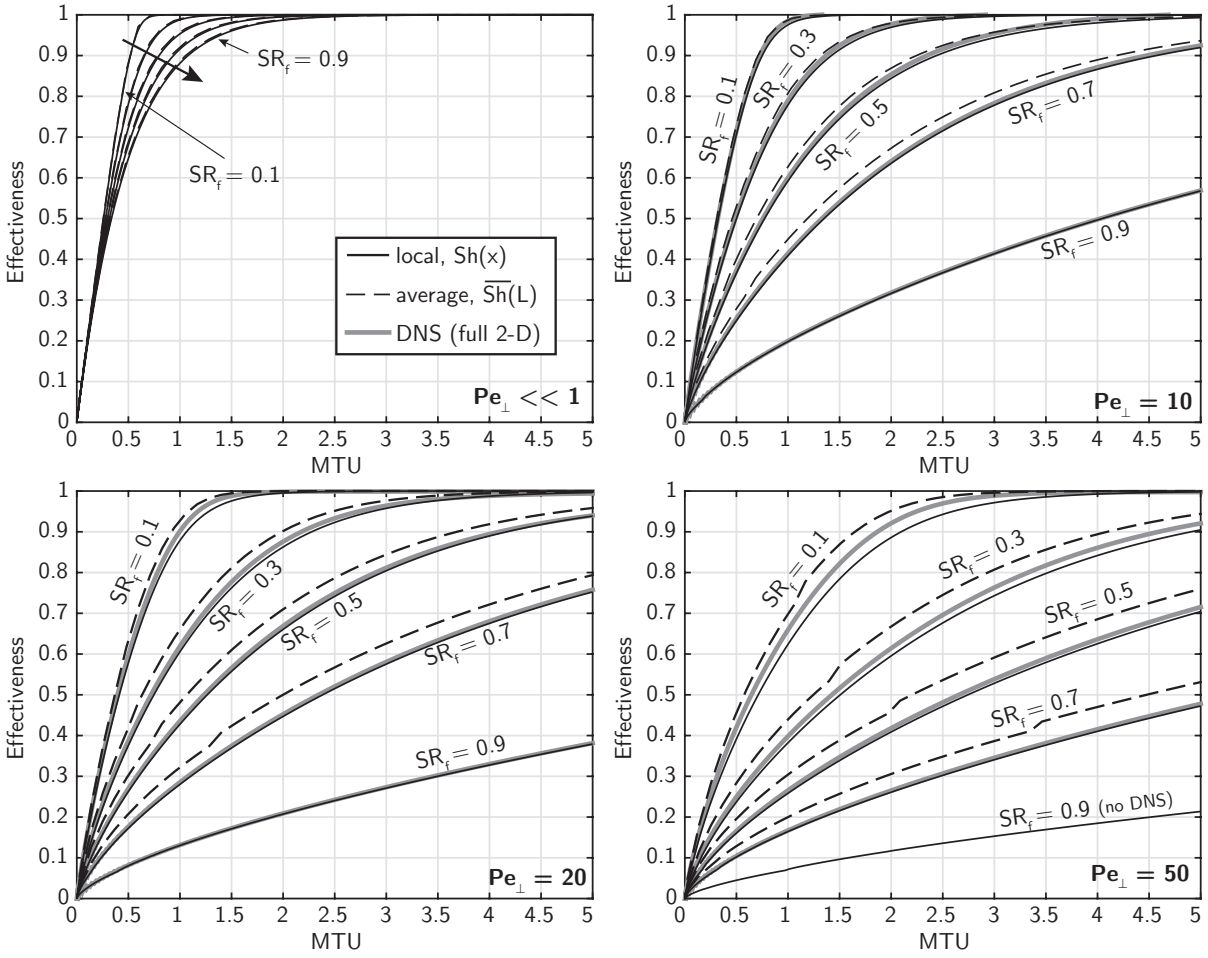

Figure 6: ε–MTU curves for increasing values of the transverse Peclet number, $\mathrm{Pe}_\perp$: as the effects of CP become more significant, correctly accounting for variations in the local mass transfer coefficient becomes more important, as seen by comparison to DNS and traditional, average Sh modeling approaches (classical stagnant film model). The present model (local) agrees well with results from DNS over the entire parameter (MTU, $\mathrm{SR_f}$, $\mathrm{Pe}_\perp$) space, but the average Sh approach breaks down for high $\mathrm{Pe}_\perp$. Kinks in the dotted lines correspond to non-smooth breaks in the correlation for $\overline{\mathrm{Sh}}$ (Eq. (46)).

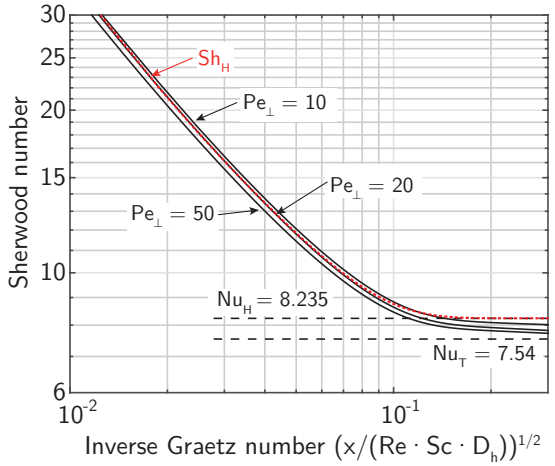

Figure 5: The local Sherwood number for various transverse Peclet numbers from direct numerical simulation shows the $1/3$ Graetz scaling that characterizes developing laminar flow is valid for a range of typical transverse Peclet numbers. Despite the permeate mass loss, the Sh still trends to a near constant for developed flow. The red curve shows the classical Graetz solution for a constant wall flux, which limits to an upper bound on the DNS results. Note that all curves converge to a value that is located between the constant value (for Nu_T, uniform wall temperature) and constant gradient (for Nu_H, constant heat flux) boundary conditions.

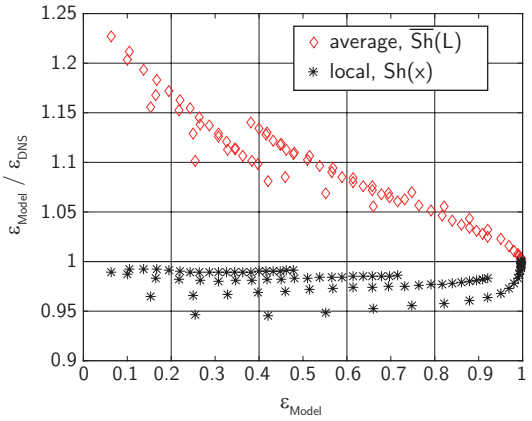

Figure 7: Relative deviation of the reduced model solutions based on the direct numerical simulation results for $Pe_\perp = 50$ and $SR_f = [0.1; 0.3; 0.5; 0.7]$. The average Sh model generally tends to overpredict the effectiveness, whereas the local Sh model (the present work) tends to underpredict effectiveness. For low effectiveness values, the overprediction of the average Sh model can exceed 20%, whereas the local Sh model does not deviate from the DNS results by more than 6%. The agreement between DNS results and the local Sh model also increases for higher values of SR_f.

a smaller solute diffusivity, which increases the mass transfer resistance. Both of these effects retard the permeate flux across the membrane, meaning a larger MTU (reflected by a greater length or length times permeability) is required to achieve high ε.

5.2. Comparison to Fully Resolved Numerical Simulations

In order to validate the model and its approximations (as discussed in Sec. 3.2), we compare the model results to solutions obtained via direct numerical simulation (DNS). Two-dimensional DNS of a stationary empty channel flow are conducted by the finite volume method employed in the open-source software package OpenFOAM[2]. More details on the method can be found in [25]. The stationary continuity, species conservation, and momentum equations are solved with the SIMPLE algorithm (Semi-Implicit Method for Pressure Linked Equations) in the entire two-dimensional channel for the boundary conditions outlined in Sec. 3.1. A constant pressure gradient between channel inlet and out-

[2] www.openfoam.org

let is applied, resulting in a parabolic, developed velocity profile at the channel inlet. Owing to the boundary condition for the velocity at the membrane surface, the flow rate (and Reynolds number) in the feed channel decrease along the channel length. Consistent with the other models in this work and elsewhere in literature, constant fluid properties were used, which has been shown to have a small effect on the results [15].

As seen in Figs. 6 and 7, the agreement between the present model and the DNS results confirms that the simplifications in the analogy to convective heat transfer (Sec. 3.2) hold for a wide range of typical RO operating conditions and geometries, deviating from DNS results by a maximum of 6%. Disagreement is generally worst at high recovery ratios (high ε, low SR_f), where feed velocity changes significantly along the channel length, and the approximation of constant u_x begins to break down. However, at large RR and MTU, the MTBL becomes developed, and Sh becomes independent of Re; in these cases the neglect of corrections to the streamwise velocity is no longer relevant. This provides evidence that the present model is valid outside the limitation stated by Eq. (21).

5.3. Comparison to Average Sh Models

The dashed lines in Fig. 6 show the ε–MTU relationship for a constant (average) Sh. As is typical in many RO models, this approach incorrectly combines an average mass transfer coefficient with a local logarithmic concentration driving force to evaluate the effects of CP. Such an approximation is only valid when the mass transfer coefficient does not vary significantly along the streamwise coordinate, which is not the case for a developing MTBL. For a constant, average Sh, the ε–MTU relationship reduces to (see Eq. (43))

$$d\varepsilon = \left[1 - \frac{\exp\left(\mathrm{Pe}_\perp \big/ \overline{\mathrm{Sh}}\right)\mathrm{SR}_f}{1-\varepsilon(1-\mathrm{SR}_f)}\right]\frac{d\mathrm{MTU}}{1-\mathrm{SR}_f}, \tag{45}$$

where

$$\overline{\mathrm{Sh}} = \begin{cases} 2.236 x_*^{-1/3}, & \text{for } x_* < 0.001, \\ 2.236 x_*^{-1/3} + 0.9, & \text{for } 0.001 \le x_* < 0.01, \\ 8.235 + 0.0364/x_*, & \text{for } x_* \ge 0.01. \end{cases} \tag{46}$$

is the Sherwood number relationship presented in [19].

As the effects of CP increase at higher $\mathrm{Pe}_\perp$, the disagreement between the average Sh model and the DNS results increase, up to a maximum of 20% at $\mathrm{Pe}_\perp = 50$. As shown in Fig. 7, the present model is in better agreement with the DNS results at these higher $\mathrm{Pe}_\perp$, where capturing the variation in Sh becomes more important. This disagreement is a consequence of a fundamental mismatch: an average mass transfer coefficient cannot be used with a local driving force to accurately compute a local flux. The apparent predictive ability of this approach at low $\mathrm{Pe}_\perp$ and SR_f is only a consequence of the smaller effects of CP on overall performance under those conditions.

5.4. Comparison to experimental data

In addition to DNS results, we validate the present model against the experimental data of Song and Tay [26]. In their experimental study, a system of commercial RO elements (ESPA-2540) was investigated. Owing to their investigated RO system, two important aspects have to be considered in the modeling process.

The membrane resistance provided by Song and Tay relates the local driving pressure difference to the local permeate flux. The permeate flux is linked with the equation of salt conservation to the local salt concentration. However, in this direct relation a factor of two (see Eq. (34)) is missing, which accounts for the spiral wound membrane, where each feed channel is confined by two membrane walls. Thus, the one-side membrane resistance is twice the resistance given in their paper. The definition of the membrane resistance has no influence on model results without concentration polarization. However, the redefined membrane resistance decreases the local permeate flux and thus the effect of concentration polarization.

A further important aspect in modeling concentration polarization of a membrane system is the modular design. The experimental system consisted of four spiral wound RO elements, each of 1 m in length (ESPA-2540). The membrane modules are connected but the intermediate section allows for mixing, such that the development of the concentration boundary layer restarts at the beginning of each element.

Figure 8 shows the model results in comparison to experimental data for three different feed velocities and a range of applied pressures. The dashed lines correspond to model results without the effect of CP, which coincide with model results presented in their study. Including the effects of CP, we obtain the thick solid line (four separate membrane modules) and the dotted line (one 4 m long membrane module). Although model results without CP fit already well with the experimental data, a better agreement is obtained if CP is accounted for.

Figure 9 reveals the effect of multiple membrane modules by showing the local decrease in permeate flux over the length of the module. For the single membrane

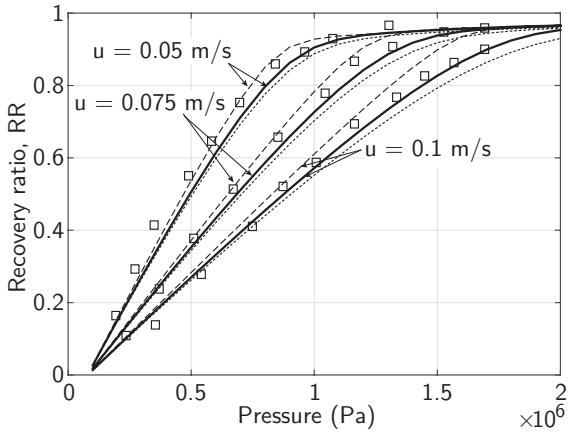

Figure 8: Comparison to experimental data from Song and Tay [26]. Experimental recoveries (symbols) and model results with (solid lines) and without (dashed lines) the effect of CP. The effect of multiple membrane modules is shown by the dotted line which illustrates one four meter long RO membrane module without intermediate interruptions.

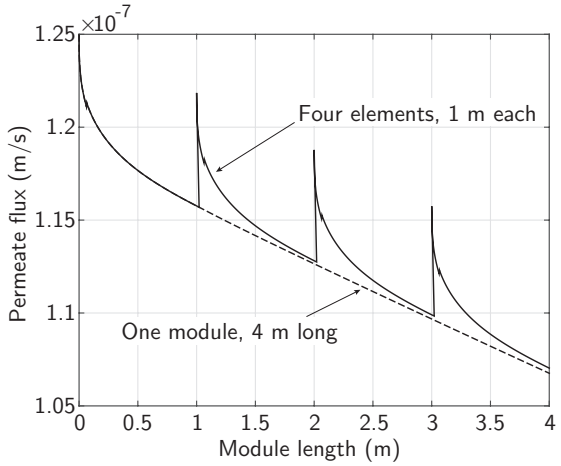

Figure 9: Effect of boundary layer renewal by multiple stages for $\Delta p = 15 \cdot 10^5$ Pa and $u = 0.05$ m/s: the average permeate flux is significantly higher when the mass transfer boundary layer is destroyed between elements.

module, the permeate flux decreases continuously as a result of increasing concentration boundary layer and the increasing bulk concentration. For the four modules of one meter each, the permeate flux exhibits sudden jumps caused by the renewing concentration boundary layer. Due to the increase in bulk concentration, the permeate flux generally decreases along flow direction.

5.5. Limitations in spacer-filled channel flows

The theoretical approach developed in this study using the principle of superposition is generally valid if the equation governing mass transfer is linear. This does not limit the approach to laminar or stationary flows. Further, a previous study showed that the classical Graetz scaling for the mass transfer entrance length is also valid for spacer-filled channels if the flow is stationary; this scaling behavior loses validity with the onset of temporal oscillations in the flow field [25]. As such, correlations for the local Sherwood number (required for the present model) in spacer-filled channels are more specific to individual channel designs. The identification of self-similarities in the transitional region (beyond the onset of oscillatory flow) is thus an important step in modeling real membrane processes with spacer-filled channels.

5.6. Consequences for High Permeability RO

As ultrapermeable membranes continue to be developed in an effort to reduce the fixed and operating costs of RO, the mass transfer resistance across the membrane will decrease. Consequently, concentration polarization will become a more dominant resistance—and thus source of inefficiency—in RO systems. Accurate modeling of CP at higher permeabilities is thus critical to optimizing performance in these new systems [3].

6. Conclusions

In this study, we have developed a new model for reverse osmosis element sizing and rating with a more fundamental basis than existing models that use empirical correlations for solute mass transfer coefficients. Using Zydney's transformation of the species equation, the solute b.c. reduces to a simpler Neumann boundary condition, similar to the energy equation in convective heat transfer with an imposed wall heat flux. We derive three dimensionless constraints that determine when this analogy between solute mass transport and convective heat transfer holds, and use the superposition theorem to account for streamwise variations in permeate flux.

The resulting integral model is benchmarked against direct numerical simulation (DNS) and experimental data. We find good agreement between the present model and both benchmarks. The model is also compared to a typical RO modeling approach that uses a single, average mass transfer coefficient like the stagnant film model. Here, we find the present model predicts DNS results better than models using an average mass transfer coefficient, particularly for high permeate fluxes. This has important implications for proposed new RO systems with ultra-permeable membranes (UPM), where CP will become a more dominant effect in limiting system performance and traditional modeling approaches break down.

Acknowledgments

The authors would like to acknowledge Leonardo Banchik for helpful discussions regarding the ε–MTU model. This work was supported by a fellowship of WR within the Postdoc-Program of the German Academic Exchange Service (DAAD). GPT and JHL thank the King Fahd University of Petroleum and Minerals for funding the research reported in this paper through the Center for Clean Water and Clean Energy at MIT and KFUPM under project number R13-CW-10.

Appendix A. Principle of superposition

To illustrate the principle of superposition, we solve for the steady-state temperature distribution of a channel flow heated by an imposed, non-uniform boundary heat flux. First, consider the case of a step change in the boundary condition (Figure A.10): the wall heat flux jumps from q_A to $q_B = q_A + \delta q$ at the location x_0. For $0 < x < x_0$, the temperature field ΔT_A is the solution to the energy equation for a uniform heat flux q_A (light grey area). For the known solutions to b.c.'s q_A and δq, the relationship between heat flux and temperature is

$$q_{\mathrm{A}} = h_{\mathrm{A}} \Delta T_A \tag{A.1}$$

$$\delta q = h_{\delta q} \Delta T_{\delta q} \tag{A.2}$$

The local heat transfer coefficient h depends on the coordinate x and the onset of the heat flux (0 for q_{A} and x_0 for δq).

Because the energy equation is linear, we can obtain the temperature at any position $x > x_0$ by adding the solution for the incremental (uniform) heat flux δq to the solution for q_A. Then, for $x > x_0$, the overall temperature difference ΔT, as shown by the dotted line in the bottom plot of Fig. A.10, results from superimposing the two solutions which yields

$$\Delta T(x) = \Delta T_A(x) + \Delta T_{\delta q}(x - x_0) \tag{A.3}$$

Inserting the expressions given in Eqs. (A.1) and (A.2) into the above leads to

$$\Delta T = \frac{q_{\mathrm{A}}}{h_A} + \frac{\delta q}{h_{\delta q}} \equiv \frac{q}{\widetilde{h}} \tag{A.4}$$

The term on the right hand side introduces a definition of a local heat transfer coefficient that relates the local heat flux and driving temperature difference. Rearranging the equation above, we find

$$\widetilde{h}(x) = \frac{q_A + \delta q}{\frac{q_{\mathrm{A}}}{h_A(x)} + \frac{\delta q}{h_{\delta q}(x - x_0)}} \qquad x > x_0 \tag{A.5}$$

For the case of a continuous variation in the local heat flux described by an arbitrary function $q(x)$, the local heat transfer coefficient at the location x can be generalized to

$$\widetilde{h}(x) = \frac{\overbrace{q_0 + \int_0^x \frac{\partial q}{\partial x} d\xi}^{q(x)}}{\frac{q_0}{h_0(x)} + \int_0^x \frac{\partial q}{\partial \xi} \frac{1}{h(x-\xi)}\, d\xi} \tag{A.6}$$

which can be written in dimensionless form as a Nusselt number based on length scale L as

$$\widetilde{\mathrm{Nu}}(x) = \frac{q_0 + \int_0^x \frac{\partial q}{\partial \xi} d\xi}{\frac{q_0}{\mathrm{Nu}(x)} + \int_0^x \frac{\partial q(\xi)}{\partial \xi} \frac{1}{\mathrm{Nu}(x-\xi)} d\xi} \tag{A.7}$$

Appendix B. Zero Mass Transfer Resistance Limit

When concentration polarization effects are negligible, i.e., in the limit of zero mass transfer resistance in the feed channel, we expect the model to reduce to the ε–MTU model [21] with no concentration polarization. Beginning with Eq. (34), we take the limit as $D \to \infty$:

$$\lim_{D\to\infty} v(x) = \lim_{D\to\infty} \left\{ A\Delta P - \frac{A f_{os} w_0}{1 - \int_0^x \frac{v(\xi)}{(v)_{f,0}}\, d\xi} \times \exp\left[\frac{D_h}{\rho D} \left(\frac{v_0}{\mathrm{Sh}(x)} + \int_0^x \frac{\partial v(x)}{\partial x} \frac{1}{\mathrm{Sh}(x-\xi)}\, d\xi \right) \right] \right\}, \tag{B.1}$$

which reduces to

$$v(x) = A\Delta P - \frac{A f_{\mathrm{os}} w_0}{1 - \int_0^x \frac{v(\xi)}{(\rho v)_{f,0}}\, d\xi}. \tag{B.2}$$

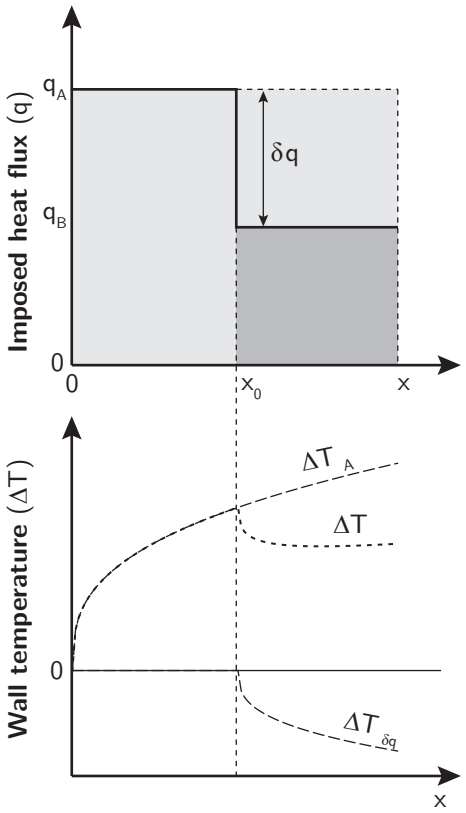

Figure A.10: Illustration of the principle of superposition applied to a heat transfer case with a spatially non-uniform heat flux.

Recasting the above in dimensionless form, using the following definitions

$$\frac{d(\mathrm{RR})}{dx} = \frac{v(x)}{v_{f,0}} \qquad \mathrm{MTU} = \frac{\Delta P\, x}{v_{f,0} H} \qquad \mathrm{SR}_f = \frac{f_{os} w_0}{\Delta P} \tag{B.3}$$

yields

$$\frac{d(\mathrm{RR})}{dx} = \frac{d(\mathrm{MTU})}{dx}\left(1 - \mathrm{SR}_f \frac{1}{1 - \int_0^x \frac{d(\mathrm{RR})}{d\xi}\, d\xi}\right), \tag{B.4}$$

or

$$d(\mathrm{RR}) = \left(1 - \frac{\mathrm{SR}_f}{1 - \mathrm{RR}}\right) d(\mathrm{MTU}), \tag{B.5}$$

which is identical to Eq. (11) in Banchik et al. [21] for the case of $\beta = 1$, i.e., no concentration polarization.

Appendix C. Transformed Momentum Equations

Conditions for the equality of the governing equations can be obtained by rewriting the conservation equations in terms of the pseudo-velocity, $\vec{u}_\omega$. The continuity equation becomes

$$\frac{\partial u_{\omega,x}}{\partial x} + \frac{\partial u_{\omega,y}}{\partial y} + D\left(\frac{\partial^2 \omega}{\partial x^2} + \frac{\partial^2 \omega}{\partial y^2}\right) = 0. \tag{C.1}$$

The momentum equation in the x-direction (the y-coordinate momentum equation is analogous) becomes

$$\begin{aligned}
&\frac{\partial u_{\omega,x}}{\partial t} + D\frac{\partial^2 \omega}{\partial x \partial t} \\
&+u_{\omega,x}\frac{\partial u_{\omega,x}}{\partial x} + D\left(\frac{\partial u_{\omega,x}}{\partial x}\frac{\partial \omega}{\partial x} + u_{\omega,x}\frac{\partial^2 \omega}{\partial x^2} + D\frac{\partial^2 \omega}{\partial x^2}\frac{\partial \omega}{\partial x}\right) \\
&+u_{\omega,y}\frac{\partial u_{\omega,x}}{\partial x} + D\left(\frac{\partial u_{\omega,x}}{\partial x}\frac{\partial \omega}{\partial y} + u_{\omega,y}\frac{\partial^2 \omega}{\partial x^2} + D\frac{\partial^2 \omega}{\partial x^2}\frac{\partial \omega}{\partial y}\right) \\
&= -\frac{1}{\rho}\frac{\partial p}{\partial x} + \frac{\mu}{\rho}\left[\frac{\partial^2 u_{\omega,x}}{\partial x^2} + \frac{\partial^2 u_{\omega,x}}{\partial y^2} + D\left(\frac{\partial^3 \omega}{\partial x^3} + \frac{\partial^3 \omega}{\partial x \partial y^2}\right)\right].
\end{aligned} \tag{C.2}$$

Solving the equations for the pseudo-velocity with the non-permeable boundary condition is strictly identical to the set of equations (3) and (6)–(8) using the permeable wall boundary condition. The additional terms of the pseudo-concentration arising in the momentum and continuity equation are corrections to the velocity field caused by the permeate flux. Introducing the local counter-diffusion velocity $v_{D,x} = D\frac{\partial \omega}{\partial x}$ and $v_{D,y} = D\frac{\partial \omega}{\partial y}$ clarifies the interpretation:

$$\begin{aligned}
&\frac{\partial u_{\omega,x}}{\partial t} + \frac{\partial v_{D,x}}{\partial t} \\
&+u_{\omega,x}\frac{\partial u_{\omega,x}}{\partial x} + \left(v_{D,x}\frac{\partial u_{\omega,x}}{\partial x} + u_{\omega,x}\frac{\partial v_{D,x}}{\partial x} + v_{D,x}\frac{\partial v_{D,x}}{\partial x}\right) \\
&+u_{\omega,y}\frac{\partial u_{\omega,x}}{\partial x} + \left(v_{D,y}\frac{\partial u_{\omega,x}}{\partial x} + u_{\omega,y}\frac{\partial v_{D,x}}{\partial x} + v_{D,y}\frac{\partial v_{D,x}}{\partial x}\right) \\
&= -\frac{1}{\rho}\frac{\partial p}{\partial x} + \frac{\mu}{\rho}\left(\frac{\partial^2 u_{\omega,x}}{\partial x^2} + \frac{\partial^2 u_{\omega,x}}{\partial y^2} + \left(\frac{\partial^2 v_{D,x}}{\partial x^2} + \frac{\partial^2 v_{D,x}}{\partial y^2}\right)\right).
\end{aligned} \tag{C.3}$$

In order to apply local or overall correlations for the transport number from the analogous solution to the convective heat transfer problem thus requires we neglect all corrections to the velocity field caused by the pseudo-concentration; i.e., all terms involving $v_{D,x}$ and $v_{D,y}$ in Eq. (C.3).

Reference

[1] T. Humplik, J. Lee, S. C. O'Hern, B. A. Fellman, M. A. Baig, S. F. Hassan, M. A. Atieh, F. Rahman, T. Laoui, R. Karnik, E. N. Wang, Nanostructured materials for water desalination, Nanotechnology 22 (29) (2011) 1–19.

[2] D. Cohen-Tanugi, J. C. Grossman, Water desalination across nanoporous graphene, Nano Letters 12 (7) (2012) 3602–3608.
[3] D. Cohen-Tanugi, R. K. McGovern, S. H. Dave, J. H. Lienhard V, J. C. Grossman, Quantifying the potential of ultra-permeable membranes for water desalination, Energy & Environmental Science 7 (3) (2014) 1134–1141.
[4] A. S. Michaels, New separation technique for the CPI, Chemical Engineering Progress 64 (12) (1968) 31–43.
[5] L. Song, M. Elimelech, Theory of concentration polarization in crossflow filtration, Journal of the Chemical Society, Faraday Transactions 91 (19) (1995) 3389–3398. doi:10.1016/0376-7388(94)00035-2.
[6] S. De, P. Bhattacharya, Prediction of mass-transfer coefficient with suction in the applications of reverse osmosis and ultrafiltration, Journal of Membrane Science 128 (2) (1997) 119–131. doi:10.1016/S0376-7388(96)00313-4.
[7] L. Song, S. Yu, Concentration polarization in cross-flow reverse osmosis, AIChE Journal 45 (5) (1999) 921–928. doi:10.1002/aic.690450502.
[8] S. Sablani, M. Goosen, R. Al-Belushi, M. Wilf, Concentration polarization in ultrafiltration and reverse osmosis: a critical review, Desalination 141 (3) (2001) 269–289. doi:10.1016/S0011-9164(01)85005-0.
[9] S. Kim, E. M. Hoek, Modeling concentration polarization in reverse osmosis processes, Desalination 186 (1–3) (2005) 111–128. doi:10.1016/j.desal.2005.05.017.
[10] D. E. Wiley, D. F. Fletcher, Techniques for computational fluid dynamics modelling of flow in membrane channels, Journal of Membrane Science 211 (1) (2003) 127–137. doi:10.1016/S0376-7388(02)00412-X.
[11] R. Ghidossi, D. Veyret, P. Moulin, Computational fluid dynamics applied to membranes: State of the art and opportunities, Chemical Engineering and Processing: Process Intensification 45 (6) (2006) 437–454. doi:10.1016/j.cep.2005.11.002.
[12] V. Geraldes, M. D. Afonso, Generalized mass-transfer correction factor for nanofiltration and reverse osmosis, AIChE journal 52 (10) (2006) 3353–3362. doi:10.1002/aic.10968.
[13] A. Subramani, S. Kim, E. M. Hoek, Pressure, flow, and concentration profiles in open and spacer-filled membrane channels, Journal of Membrane Science 277 (1) (2006) 7–17. doi:10.1016/j.memsci.2005.10.021.
[14] A. L. Zydney, Stagnant film model for concentration polarization in membrane systems, Journal of Membrane Science 130 (1–2) (1997) 275–281. doi:10.1016/S0376-7388(97)00006-9.
[15] E. Lyster, Y. Cohen, Numerical study of concentration polarization in a rectangular reverse osmosis membrane channel: Permeate flux variation and hydrodynamic end effects, Journal of Membrane Science 303 (1–2) (2007) 140–153. doi:10.1016/j.memsci.2007.07.003.
[16] J. M. Miranda, J. B. Campos, An improved numerical scheme to study mass transfer over a separation membrane, Journal of Membrane Science 188 (1) (2001) 49–59. doi:10.1016/S0376-7388(01)00360-X.
[17] A. Bejan, Convective Heat Transfer, John Wiley & Sons, Inc., 2013.
[18] W. M. Kays, M. E. Crawford, Convective Heat and Mass Transfer, McGraw-Hill, 1987.
[19] R. K. Shah, A. L. London, Advances in Heat Transfer – Laminar flow forced convection in ducts: A source book for compact heat exchanger analytical data, Academic Press, New York, 1978. doi:10.1016/B978-0-12-020051-1.50001-2.
[20] J. G. Wijmans, R. W. Baker, The solution-diffusion model: a review, Journal of Membrane Science 107 (1995) 1–21.
[21] L. D. Banchik, M. H. Sharqawy, J. H. Lienhard V, Effectiveness-mass transfer units (ε–MTU) model of a reverse osmosis membrane mass exchanger, Journal of Membrane Science 458 (2014) 189–198. doi:10.1016/j.memsci.2014.01.039.
[22] S. C. Chapra, R. P. Canale, Numerical Methods for Engineers, McGraw-Hill, 2006.
[23] C. Koutsou, S. Yiantsios, A. Karabelas, A numerical and experimental study of mass transfer in spacer-filled channels: Effects of spacer geometrical characteristics and Schmidt number, Journal of Membrane Science 326 (1) (2009) 234–251. doi:10.1016/j.memsci.2008.10.007.
[24] J. H. Lienhard IV, J. H. Lienhard V, A Heat Transfer Textbook, 4th Edition, Dover Publications, 2011.
URL `http://ahtt.mit.edu`
[25] W. Rohlfs, J. H. Lienhard V, Entrance length effects on Graetz number scaling in laminar duct flows with periodic obstructions: Transport number correlations for spacer-filled membrane channel flows, International Journal of Heat and Mass Transfer 97 (2016) 842–852.
[26] L. Song, K. G. Tay, Performance prediction of a long crossflow reverse osmosis membrane channel, Journal of Membrane Science 281 (1–2) (2006) 163–169. doi:10.1016/j.memsci.2006.03.026.